Complex Industrial Machinery Health Diagnosis Challenges and Strategies

Hsiao-Yu Wang(✉) and Ching-Hua Hung

Department of Mechanical Engineering, National Yang Ming Chiao Tung University, Hsinchu City 300093, Taiwan
shon0808@gmail.com

Abstract. This study is dedicated to addressing a spectrum of pivotal challenges and predicting their potential ramifications. Specifically, its objectives encompass the detection of tool breakage in milling-turning composite machinery, the assessment of the service life of punching machine heads, and the evaluation of mold longevity in forging apparatus, among other intricacies. The overarching objective is the establishment of an equipment health diagnosis system tailored for intricate industrial setups. It is evident from our interactions with the industry that the rationale for monitoring strategies and threshold values are contingent upon the idiosyncratic attributes of the equipment and the sector. While the metal processing sector has been trailing behind the semiconductor industry in the realm of intelligent monitoring by an approximate span of a decade, it faces an analogous array of challenges. These encompass dwindling demographics, leading to an increased reliance on external labor for shifts, elevated personnel turnover rates thereby limiting the availability of experienced personnel for tasks such as tool changes, mold replacements, and maintenance. Additionally, the necessity to uphold traceability standards for mold and punching head usage history, notably in the context of aerospace industry compliance, compounds these challenges. Consequently, the industry aspires to achieve two paramount objectives for vital production equipment: first, the execution of failure diagnostics to appraise tool or mold longevity and assess product quality. Second, the transition from time-based to condition-based maintenance practices, even under conditions that necessitate frequent mold substitutions to cater to diverse product manufacturing needs.

Keywords: Root Mean Square · Statistical overlap factor · Ensemble Empirical Mode Decomposition · Bayesian regularization

1 Introduction

Piercing processes are extensively used in stamping products, often equipped with up to 24 die sets. However, varying levels of wear due to uneven loading, machining tolerances, and assembly factors pose significant challenges. When a die fails, it necessitates the removal of molds for die replacement. Systematically assessing the remaining lifespan of other dies and replacing them simultaneously could reduce production losses

D.-J. Deng and J.-C. Chen (Eds.): SGIoT 2023, LNICST 557, pp. 130–140, 2024.
https://doi.org/10.1007/978-3-031-55976-1_13

during mold changeovers. The theoretical challenges lie in unfavorable signal-to-noise ratios in factory environments, minimal stiffness variations in micro-die structures, and disturbances from rigid body modes in signals, all of which affect failure diagnosis outcomes.

Stamping processes are highly nonlinear transient procedures. Developing knowledge-experience-based solutions often results in non-generic, case-specific monitoring systems. Additionally, the time-consuming process of establishing the learning curve for these monitoring systems is a concern. The research focus of our team includes the proper decoupling of fault characteristics or signals and their selection as indicators of machine health status in low-sample learning scenarios.

2 Materials and Methods

This study focuses on constructing a monitoring system for a C-frame punch press, targeting two main objectives: 1) abnormal machine operation vibration detection, and 2) abnormal detection of tools (such as dies and punch heads) in the stamping process. The monitoring positions planned by our team are illustrated in Fig. 1.

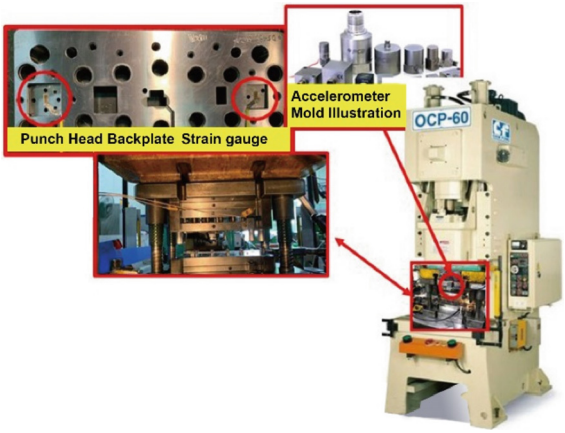

Fig. 1. Sensor Planning Illustration Diagram

An accelerometer device is installed on the crankshaft assembly for long-term monitoring, allowing observation of any misalignment or wear in the crankshaft and bushing. However, for shorter-term monitoring, it is utilized to observe abnormal vibrations in the mold during stamping, providing insights into punch head wear issues. The actual on-site installation is shown in Fig. 2.

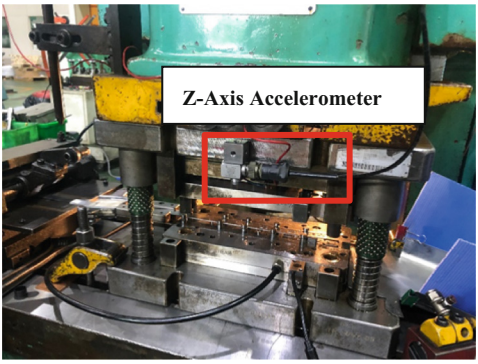

Fig. 2. On-Site Sensor Installation Diagram

Another monitoring position involves embedding sensors into the backplate of the mold, as depicted in Fig. 3. The backplate, being a direct force-bearing component in the punch head, serves as an excellent source of signals for studying punch head wear. Strain gauges, replacing costlier load cells, are predominantly used in the backplate. These strain gauges are installed through structural design and calibrated to convert strain signals into tonnage values. Changes in tonnage values during forming are observed concerning the original strain signals. The study has also verified the relationship between punch head wear and the forces exerted on the backplate and machine vibrations.

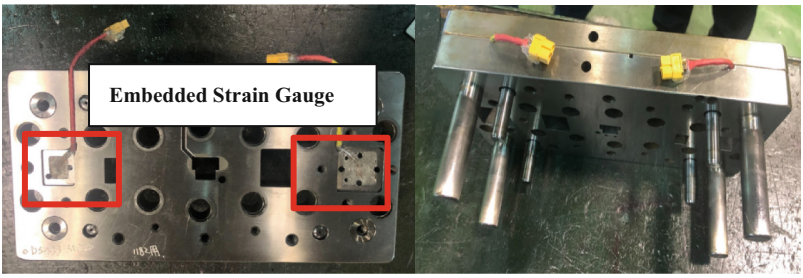

Fig. 3. Post-Installation Configuration Diagram on the Die

The key sensor trigger timing is facilitated by a digital encoder installed on the machine's crankshaft, significantly reducing post-signal processing tasks such as signal stitching and eliminating unnecessary signals. During the initial stages of research, on-site technicians use our designed app to annotate abnormal time points, such as punch head fractures, mold abnormalities, and machine anomalies. This practice narrows down the range for identifying signal differences and accelerates signal labeling until the algorithm effectively extracts identifiable abnormal signals.

The subsequent sections will provide a detailed description of the monitoring system's planning, including hardware (sensors, signal processors, signal extractors, industrial computers) and software (monitoring system platform).

2.1 Hardware Measurement Architecture

The hardware configuration utilizes sensors that provide analog signal output. These analog signals are coupled with a signal conditioner (SC) to provide IEPE (Integrated Electronics Piezoelectric) power to the accelerometers. The signal conditioner also serves to preprocess the signals, including filtering out any power disturbances originating from the factory environment. Subsequently, the analog signals are converted to digital signals using a Data Acquisition (DAQ) system.

For the accelerometers, a 16-bit Analog to Digital Converter (ADC) is employed for data conversion. In the case of strain gauges, a high-specification 24-bit ADC is utilized, enabling precise measurement of metal deformation down to a strain level of $(10)^{-6}$.

The two depicted snapshot cards represent physical signal lines that connect to a Data Acquisition (DAQ) unit, which is then connected to the monitoring system on the computer. The monitoring system is designed to accommodate both wireless Wi-Fi and physical Ethernet network connections, depending on the actual on-site configuration.

In terms of software design, it is customized to meet the specific requirements of Company A. The interface includes a homepage displaying key statistics such as machine utilization rates and the actual number of completed stamping operations. This information is presented in a way that is easily understandable for on-site personnel. The subsequent pages provide real-time reception of the raw signals, allowing our personnel to monitor the status of signal lines and hardware for any anomalies or irregularities.

2.2 Methods

In related research, our team has achieved preliminary results in monitoring the lifespan of single punching heads in the punching process. In the findings presented in [5], it was confirmed that through time analysis and frequency analysis, the extracted feature signals could establish a correlation between punching head wear and burr height. In [6], a logistic regression analysis and the use of the statistical overlap factor were employed to assess the logical thresholds for decision-making in the monitoring system. All of these experimental and analytical research outcomes were conducted using a 50-ton hydraulic punching machine in our university's smart factory.

In terms of software design, it is customized to meet the specific requirements of Company A. The interface includes a homepage displaying key statistics such as machine utilization rates and the actual number of completed stamping operations. This information is presented in a way that is easily understandable for on-site personnel. The subsequent pages provide real-time reception of the raw signals, allowing our personnel to monitor the status of signal lines and hardware for any anomalies or irregularities.

2.3 Process

The signal explanation in Fig. 4 is derived from our team's research on stamping processes and the reference [4]. A complete stamping vibration signal is divided into three phases based on the relative time corresponding to the stamping machine's stroke:

1. Upper Die Pressing Stage: The phase when the upper die presses the material.
2. Punching Stage: The phase when the punch pierces through the material.
3. Upper Die Lifting Stage: The phase when the upper die is lifted.

By conducting statistical comparisons in the referenced study, it was determined that the vibration signal during the punching stage provides more accurate characteristics of the actual stamping process. It was also confirmed that there is a positive correlation between punch wear and the vibration during the punching stage.

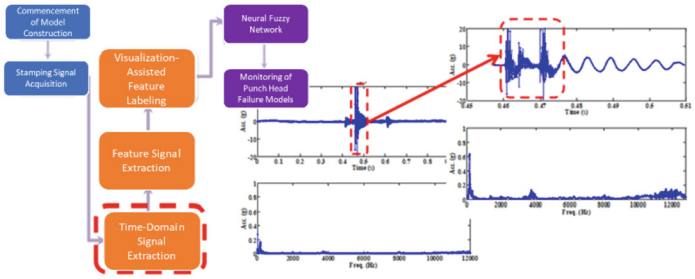

Fig. 4. Research Process Diagram - Time-Domain Signal Extraction

In Fig. 5, an explanation of the measured vibration and strain signals in an actual company B stamping plant is provided. By measuring the z-axis vibration using an accelerometer, the signals during a complete punching process can be divided into four signal amplitudes, corresponding to the following stages:

1. **Bed Movement:** The upper bed moves downward from the top.
2. **Die Pressing Stage:** The vibration signal generated when the pressing plate first contacts the sheet metal and the lower die.
3. **Punching Stage:** The moment when the punch extends downward to pierce the sheet metal.
4. **Lifting Stage:** After the punching is complete, the upper bed moves upward, and the pressing plate disengages from the sheet metal.

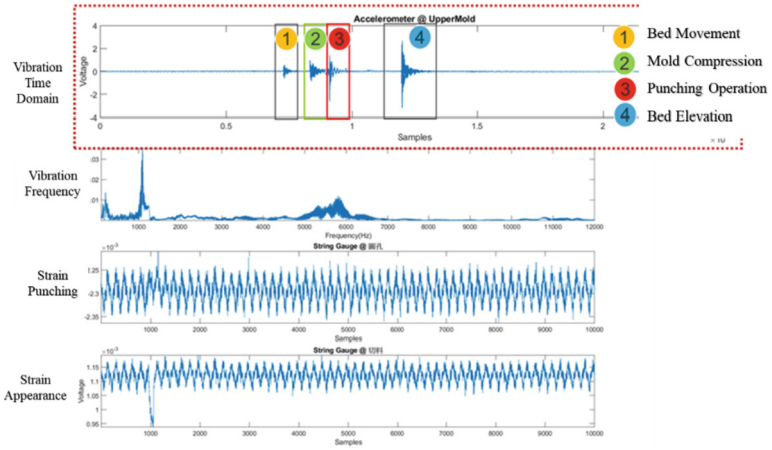

Fig. 5. Time-Domain Signal Extraction Explanation Diagram

Based on the signal extraction process, the third stage, the punching stage, is isolated, as shown in Fig. 6. From top to bottom, the figure displays the punching stage in the time domain vibration, frequency domain vibration, punch strain, and external strain, completing a time-domain extraction process. The following will explain the overall number of experiments and how each punching event is converted into energy values to compare their differences.

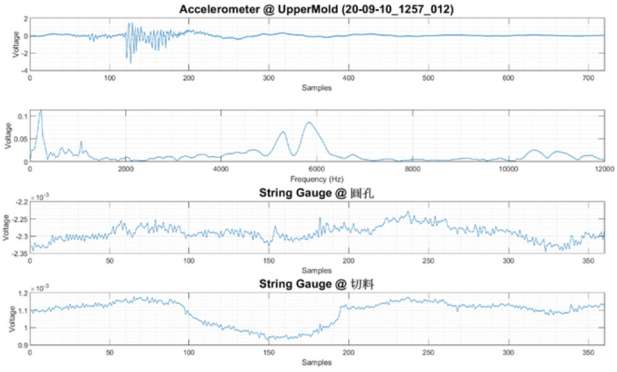

Fig. 6. Time-Domain Signal Extraction - Punching Segment Signal Diagram

Based on the signal extraction process, the third stage, the punching stage, is isolated, as shown in Fig. 6. From top to bottom, the figure displays the punching stage in the time domain vibration, frequency domain vibration, punch strain, and external strain, completing a time-domain extraction process. The following will explain the overall number of experiments and how each punching event is converted into energy values to compare their differences.

In this research, the energy statistics method used is the Root Mean Square (RMS), as shown in Eq. 1. It converts the extracted vibration and strain values into representative numerical quantities, effectively illustrating how the values change as the number of stamping cycles increases over time. In this experiment, as presented in Table 1, there were a total of 15,410 data points, with 3,044 data points in the stamping range of 1–5 k cycles and 12,366 data points in the range of 25 k–46 k cycles.

$$\text{Root Mean Square (RMS)} : x_{rms} = \sqrt{\frac{\sum_{n=1}^{N} x(n)^2}{n}} \tag{1}$$

Table 1. Stamping Experiment Data.

Item Interval	Stamping Interval (Cycles)	Number of Data Points (Entries)
1	1–5 k	3,044
2	25 k–46 k	12,366

Figure 7 consists of upper and lower panels, each displaying the time-domain and frequency-domain vibration signals after extraction. The energy trends, calculated using the RMS method, are also presented. Both sets of data from the two stamping intervals are overlaid for comparison. From these two panels, it can be observed that for the 25 k–46 k (cycles) interval, approximately 50% of the values fall near the maximum values of 0.4 (time-domain value chart) and 0.03 (frequency-domain value chart). Conversely, for the 1–5 k (cycles) interval, there are no values near the maximum. In this context, the original time-domain and frequency-domain values show only minor differences. Further feature signal extraction using the EEMD method is required to represent the magnitude of the increase in the stamping interval values.

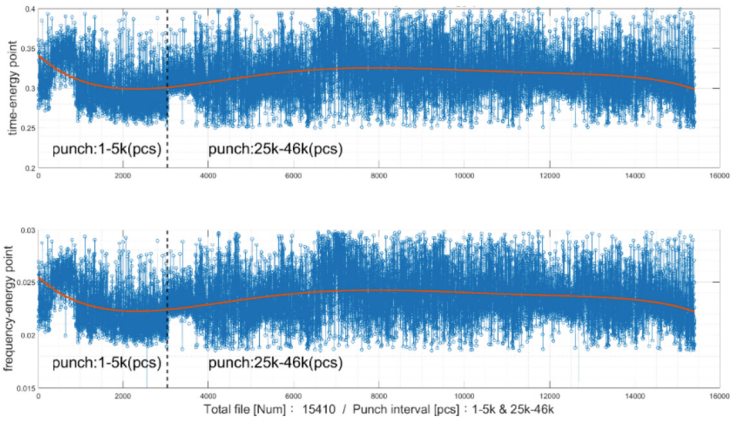

Fig. 7. Illustrates the vibration energy chart, with the upper panel displaying time-domain energy values and the lower panel showing frequency-domain energy values.

Figure 8 depicts the strain signals extracted from the punching and appearance forming processes, with the upper panel showing the strain signal from the punching process and the lower panel displaying the strain signal from the appearance forming process. The strain sensor behind the punch can most directly reflect the stress conditions and wear level of the punch during the punching process. In the upper panel, the strain signal from the punching process exhibits linear growth, increasing from $2.3 * 10^{-3}$ *to* $2.125 * 10^{-3}$ between intervals 1 and 2. In contrast, the lower panel shows the strain signal from the appearance forming process increasing from $1.1 * 10^{-3}$ *to* $1.35 * 10^{-3}$. The strain linearity in the appearance punch head is less pronounced compared to the punching punch head, primarily due to differences in punch head shape and dimensions, as illustrated in Fig. 9. The left image in Fig. 9 shows a circular punching punch head, while the right image depicts a concave appearance punch head, highlighting the observed differences.

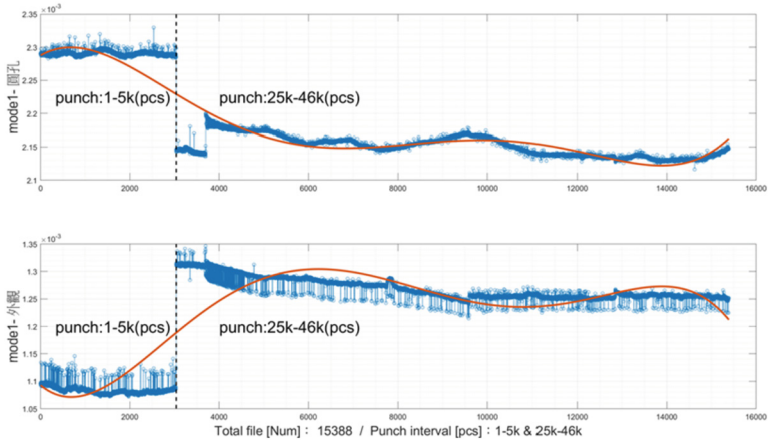

Fig. 8. Displays the strain energy charts, with the upper chart representing the values from the punching forming process, and the lower chart representing the values from the appearance forming process.

- Ensemble Empirical Mode Decomposition (EEMD): [1, 2, 3] The Hilbert-Huang Transform (HHT), proposed by Dr. Norden E. Huang and his colleagues in 1998, consists of two main steps: Empirical Mode Decomposition (EMD) and Hilbert Transform (HT). The Ensemble Empirical Mode Decomposition (EEMD) used in this study, also introduced by Dr. Norden E. Huang in 2008, aims to improve the Intrinsic Mode Functions (IMF) extracted in the EMD process.

In EMD, it is essential that both local maxima and local minima cross zero points. If an extremum does not cross a zero point, it is ignored, and the next extremum at a zero crossing is taken. This may lead to the extraction of amplitudes larger than the original signal, causing signal distortion. To prevent this distortion, EEMD adds white noise with minimal amplitude, satisfying Gaussian processes, to the time-domain signal

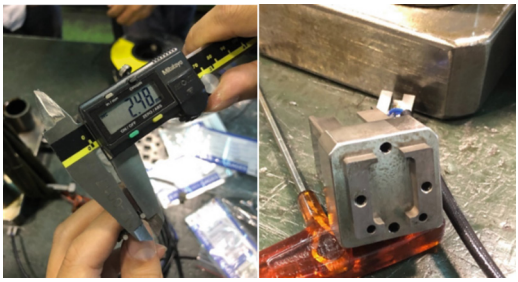

Fig. 9. Illustrates the schematic diagrams of the punch head dimensions, with the left diagram depicting the circular punch head for punching, and the right diagram representing the concave-shaped appearance punch head.

before processing. This creates an ensemble of multiple samples, and the true IMF is defined as the average of the samples obtained through EMD.

Figure 10 shows the vibration signal from the 24th stamping cycle in the Shunde on-site stamping process, subjected to the EEMD decomposition process. The X-axis represents data points, and the Y-axis represents vibration values. The signal is decomposed into eight IMF components, with the frequency decreasing from IMF1 (high-frequency) to IMF8 (low-frequency). These eight IMFs are considered as significant features, and after statistical analysis, they are used as input parameters to construct the punch head failure monitoring model.

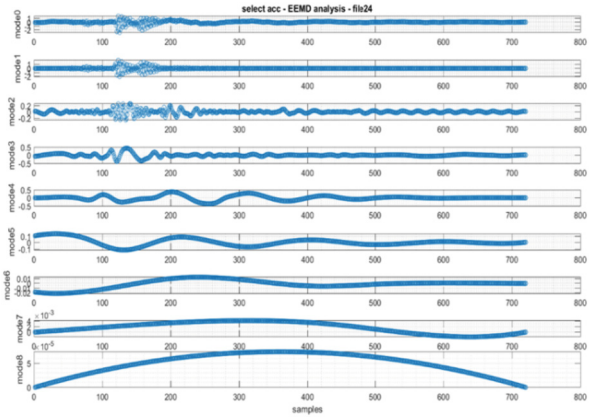

Fig. 10. EEMD Decoupling of Accelerometer Vibration Signals

Figure 11, we employ Eq. (1) to perform statistical calculations for EEMD (Ensemble Empirical Mode Decomposition) modes 1 through 8 within two distinct stamping intervals, delineated by the black dashed lines. These intervals correspond to the stamping ranges specified in Table 1, specifically, 1–5 k strokes and 25 k–46 k strokes. The X-axis in the figure represents a total of 15,410 data points of stamping records, while the Y-axis represents the vibration energy values obtained through RMS (Root Mean

Square) analysis of each stamping event. From top to bottom, the plot presents the energy values for EEMD modes 1 through 8.

Mode 1, representing the original time-domain signal, exhibits minimal differences in values between the two intervals, making it unsuitable for use as an input parameter. Modes 2 to 4, however, clearly demonstrate noticeable variations in values, rendering them highly suitable as the primary parameters for training. Modes 5 to 8 exhibit moderate differences in values and can also be employed as supplementary training data.

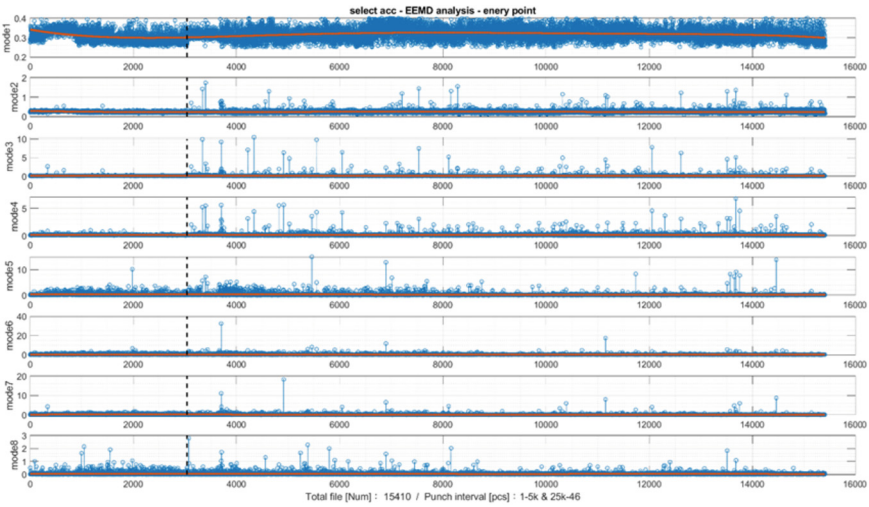

Fig. 11. Vibration Energy Representation of EEMD Mode 1 – Mode 8

- Neural Network Model (Bayesian regularization, BR): The Bayesian regularization (BR) algorithm serves as the foundation for the model used in this research, aiming to expedite the training speed of neural networks. The Bayesian regularization method is specifically designed to utilize a mean square error loss function. As mentioned in reference [7], trainbr can train neural networks as long as network weights, inputs, and transfer functions are differentiable.

  Bayesian regularization minimizes the linear combination between the square error and the weights, modifying this combination to ensure the network's generalizability upon training completion, as discussed by Foresee and Hagan in reference [8]. The algorithm incorporates Bayesian regularization within the Levenberg-Marquardt optimization method. Backpropagation is employed to compute the performance gradient with respect to weights and bias variables, denoted as jX. Each variable is adjusted according to Levenberg-Marquardt as follows:

$$\mathrm{jj} = \mathrm{jX} * \mathrm{jX}\ \mathrm{je} = \mathrm{jX} * \mathrm{E}\ \mathrm{dX} = -(\mathrm{jj} + \mathrm{I} * \mathrm{mu})\backslash \mathrm{je},$$

  where E represents all error terms, I is the identity matrix, and mu is an adaptive value increased by mu_inc until the above change leads to a decrease in performance.

Subsequently, the network is updated, and mu is decreased by mu_dec. Training stops under the following conditions:

- Maximum number of training epochs is reached.
- Maximum training time is exceeded.
- Performance falls below a certain threshold.
- Performance gradient becomes smaller than min_grad.
- mu exceeds mu_max.

3 Conclusions

This research has successfully developed a stamping die failure monitoring model. Notably, even before the die reaches near-complete wear (around 120,000 to 180,000 strokes), the model can effectively differentiate data from 46,000 stamping cycles with an impressive 95% accuracy rate. This underscores the robustness of our signal processing methodology, which excels at extracting subtle die condition variations.

Looking ahead, the next research phase will focus on two key directions. Firstly, ongoing efforts will enhance the online AI model training process, ensuring systematic and dynamic updates. Secondly, modular AI models will be explored to address the common industrial scenario of switching between different product lines, where existing models fall short. This modular approach involves collecting clustering data during production and retaining it for subsequent analysis when producing the same product in the future.

This research represents a significant leap in stamping die monitoring capabilities, enabling accurate prediction of complete die lifespan, and contributing to enhanced production efficiency.

References

1. Zhidong, Z., Min, P., Yuquan, C.: Instantaneous frequency estimate for non-stationary signa. In: Fifth World Congress on Intelligent Control and Automation, vol. 4, pp. 3641–3643 (2004)
2. Ruqiang, Y., Gao, R.X.: Hilbert–Huang transform-based vibration signal analysis for machine health monitoring. IEEE Trans. Instrum. Meas. **55**, 2320–2329 (2006)
3. Yuping, Z.: Hilbert-Huang transform and marginal spectrum for detection of bearing localized defects. In: The Sixth World Congress on Intelligent Control and Automation, vol. 2, pp. 5457–5461 (2006).
4. Sari, D.Y., Wu, T.-L.: Investigation on sound signal emitted bypunching process for punch failure monitoring. In: Conference Paper Mar (2017)
5. Sari, D.Y., Wu, T.-L., Lin, B.-T.: Preliminary study for online monitoring during the punching process. Int. J. Adv. Manuf. Technol. **88**, 2275–2285 (2017)
6. Wu, T.-L., Sari, D.Y., Lin, B.-T., Chang, C.-W.: Monitoring of punch failure in micro-piercing process based on vibratory signal and logistic regression. Int. J. Adv. Manuf. Technol. **93**, 2447–2458 (2017)
7. MacKay, D.J.C.: Computation and neural systems. Neural Comput. **4**(3), 415–447 (1992)
8. Hagan F.-R.: Proceedings of the International Joint Conference on Neural Networks, June (1997)